Human Molecular Genetics, 2014, Vol. 23, No. 20 **5452–5463**
doi:10.1093/hmg/ddu270
Advance Access published on May 29, 2014

P38α MAPK underlies muscular dystrophy and myofiber death through a Bax-dependent mechanism

Erin R. Wissing[1,†], Justin G. Boyer[1,†], Jennifer Q. Kwong[1], Michelle A. Sargent[1], Jason Karch[1], Elizabeth M. McNally[2], Kinya Otsu[3] and Jeffery D. Molkentin[1,4,*]

[1]Department of Pediatrics, Cincinnati Children's Hospital Medical Center, University of Cincinnati, Cincinnati, 240 Albert Sabin Way, Cincinnati, OH 45229, USA, [2]Department of Medicine, Section of Cardiology, University of Chicago, 5841 S. Maryland, MC 6088, Chicago, IL 60637, USA, [3]Cardiovascular Division, King's College London, 125 Coldharbour Lane, London SE5 9NU, UK and [4]Howard Hughes Medical Institute, Cincinnati Children's Hospital Medical Center, Cincinnati, 240 Albert Sabin Way, Cincinnati, OH 45229, USA

Received January 10, 2014; Revised April 22, 2014; Accepted May 27, 2014

Muscular dystrophies are a group of genetic diseases that lead to muscle wasting and, in most cases, premature death. Cytokines and inflammatory factors are released during the disease process where they promote deleterious signaling events that directly participate in myofiber death. Here, we show that p38α, a kinase in the greater mitogen-activated protein kinase (MAPK)-signaling network, serves as a nodal regulator of disease signaling in dystrophic muscle. Deletion of *Mapk14* (p38α-encoding gene) in the skeletal muscle of *mdx*- (lacking dystrophin) or *sgcd*- (δ-sarcoglycan-encoding gene) null mice resulted in a significant reduction in pathology up to 6 months of age. We also generated MAPK kinase 6 (MKK6) muscle-specific transgenic mice to model heightened p38α disease signaling that occurs in dystrophic muscle, which resulted in severe myofiber necrosis and many hallmarks of muscular dystrophy. Mechanistically, we show that p38α directly induces myofiber death through a mitochondrial-dependent pathway involving direct phosphorylation and activation of the pro-death Bcl-2 family member Bax. Indeed, muscle-specific deletion of *Bax*, but not the apoptosis regulatory gene *Tp53* (encoding p53), significantly reduced dystrophic pathology in the muscles of MKK6 transgenic mice. Moreover, use of a p38 MAPK pharmacologic inhibitor reduced dystrophic disease in *Sgcd*$^{-/-}$ mice suggesting a future therapeutic approach to delay disease.

INTRODUCTION

The muscular dystrophies are a large cadre of inherited disorders that are characterized by progressive muscle weakness and wasting and, in many cases, premature death (1). The muscular dystrophies are generally caused by mutations in genes encoding proteins in the dystrophin glycoprotein complex, an oligomeric assembly that connects the cytoskeleton and contractile elements within the myofiber to the extracellular matrix, thus stabilizing the sarcolemmal membrane (1–3). Deficiencies in this complex creates instability of the sarcolemmal membrane that leads to contraction-induced microtears or activation of membrane calcium permeable channels, creating a state of calcium overload that can lead to myofiber death (2–4). Unregulated influx of calcium in combination with increased inflammatory signaling through G-protein-coupled receptors and receptor tyrosine kinases on the myofiber sarcolemmal membrane stimulates intracellular signaling that can be detrimental and initiate myofiber death (5). These signaling events lead to activation of the mitogen-activated protein kinase (MAPK) family of proteins, which includes p38 MAPK, a known regulator of death in other cell types (6–9). Given that myofiber death and muscle wasting is an integral part of the pathology of muscular dystrophy, we hypothesized that p38 MAPK could play a pathogenic role.

p38 MAPK signaling has been shown to affect some aspects of skeletal muscle development and maturation in the mouse. Specifically, the p38α isoform, which is the most prevalent isoform

*To whom correspondence should be addressed at: Cincinnati Children's Hospital Medical Center, Cincinnati, 240 Albert Sabin Way, MLC7020, Cincinnati, OH 45229, USA. Email: jeff.molkentin@cchmc.org
†E.R.W. and J.G.B. contributed equally.

expressed in skeletal muscle, can affect myoblast fusion to form myotubes (10–12). Very little is known of p38′s direct role in the pathogenesis of muscular dystrophy, although it was shown to be upregulated in exercise-trained *mdx* mice, a genetic model of Duchenne muscular dystrophy, but unchanged in wild-type (Wt) exercise-trained mice (13). Further, deletion of dual specificity phosphatase-1 (*Dusp1*), a negative regulator of p38 MAPK and c-Jun N-terminal kinase (JNK) signaling, exacerbated the dystrophic pathology in *mdx* mice by impacting regeneration, suggesting a pathologic role for p38 in the *mdx* mouse (14). However, mice lacking *Dusp10*, another negative regulator of p38 MAPK and JNK, showed improved muscle pathology in the *mdx* background suggesting that p38 signaling was protective (15). *In vitro*, phospho-p38 was induced by 2-fold after oxidative stress in *mdx*-cultured myotubes versus Wt, whereas the p38 inhibitor SB203580 improved the survival of *mdx* myofibers after oxidative stress (16). Thus, there is little direct understanding of the role that this kinase might play in affecting muscular dystrophy. Here, we show that p38 has an important role in regulating myofiber death in mouse models of muscular dystrophy through direct phosphorylation and activation of the pro-death effector Bax.

RESULTS

Muscle-specific deletion of *Mapk14* (p38α) reduces pathology in dystrophic mice

To understand the role of p38 signaling in muscular dystrophy, we first examined the activation of the p38 MAPK pathway in two mouse models of muscular dystrophy: $Sgcd^{-/-}$ mice, a model of limb-girdle muscular dystrophy type-2F, and *mdx* mice (which lack dystrophin), a model of human Duchenne muscular dystrophy. At 3 months of age, diseased skeletal muscle from $Sgcd^{-/-}$ mice showed significant hyperphosphorylation of p38 (3.9-fold ± 0.5) and its downstream target phospho-MK2 (4.1-fold ± 0.8) by western blotting (Fig. 1A). A significant increase in phospho-p38 (2.8-fold ± 0.2) and phospho-MK2 (1.9-fold ± 0.6) was also observed in skeletal muscle from *mdx* mice (Fig. 1B), collectively suggesting enhanced activation of the p38 MAPK pathway in muscular dystrophy.

To directly evaluate the role that p38α might play in muscular dystrophy, we instituted a muscle-specific loss-of-function approach in the skeletal muscle of mice using a *Mapk14-loxP*-targeted allele (fl) in combination with the muscle-specific

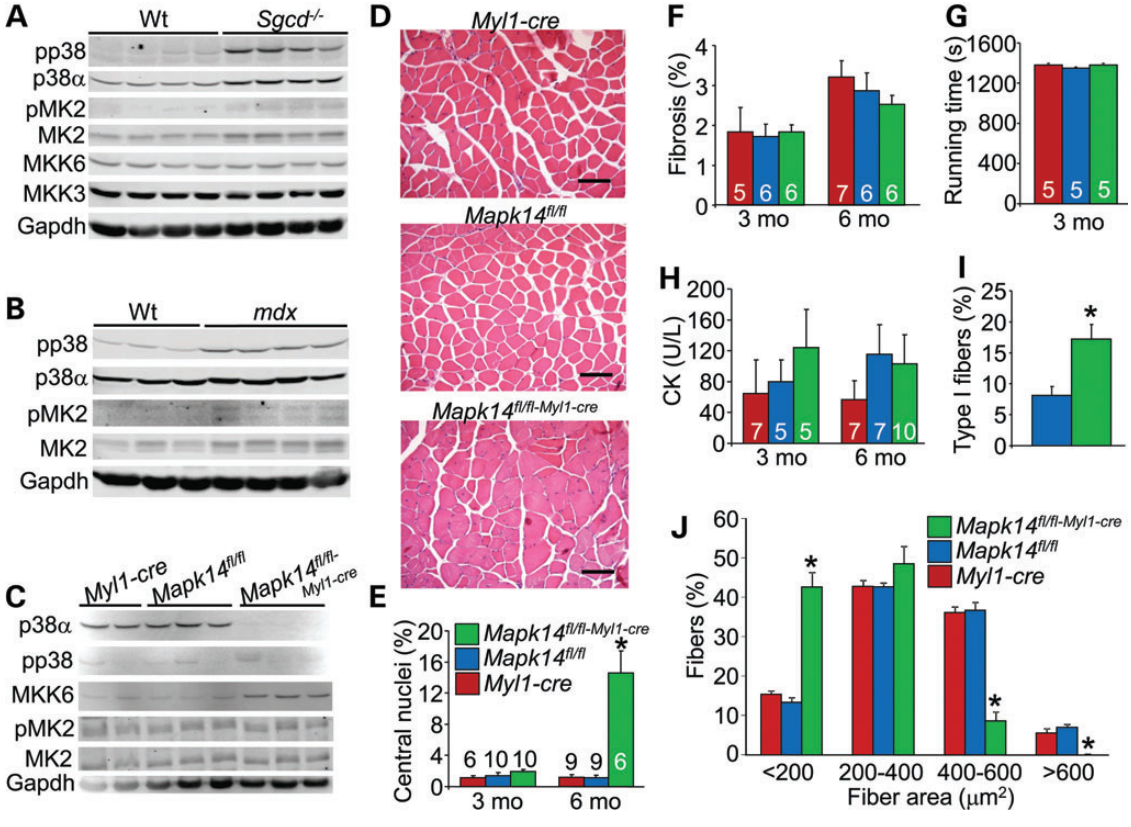

Figure 1. Baseline expression of p38 MAPK in dystrophic and Mapk14 gene-deleted mice. (**A** and **B**) Western blot for the indicated proteins from 3-month-old $Sgcd^{-/-}$ or *mdx* dystrophic quadriceps tissue. Fold increase in phospho-p38 (pp38) and that in phospho-MK2 are shown. (**C**) Western blots for the indicated proteins from 6-week-old quadriceps tissue of *Myl1-cre*, $Mapk14^{fl/fl}$ and $Mapk14^{fl/fl\text{-}Myl1\text{-}cre}$ mice. (**D**) Representative baseline histological sections stained with H&E from quadriceps of 6-week-old *Myl1-cre*, $Mapk14^{fl/fl}$ and $Mapk14^{fl/fl\text{-}Myl1\text{-}cre}$ mice. Scale bars are 100 μm. (**E**) Percentage of myofibers containing central nuclei in the quadriceps muscle of 3- and 6-month-old *Myl1-cre*, $Mapk14^{fl/fl}$ and $Mapk14^{fl/fl\text{-}Myl1\text{-}cre}$ mice, quantified from histological sections. (**F**) Percentage of fibrotic area in the quadriceps muscle of 3- and 6-month-old *Myl1-cre*, $Mapk14^{fl/fl}$ and $Mapk14^{fl/fl\text{-}Myl1\text{-}cre}$ mice, quantified from histological sections. (**G**) Average time spent running on a treadmill of 3-month-old *Myl1-cre*, $Mapk14^{fl/fl}$ and $Mapk14^{fl/fl\text{-}Myl1\text{-}cre}$ mice. (**H**) Average amount of CK found in the serum of 3- and 6-month-old *Myl1-cre*, $Mapk14^{fl/fl}$ and $Mapk14^{fl/fl\text{-}Myl1\text{-}cre}$ mice. (**I**) Quantitation of type I fibers in the quadriceps of $Mapk14^{fl/fl}$ and $Mapk14^{fl/fl\text{-}Myl1\text{-}cre}$ mice at 6 months of age. Four mice each were analyzed with greater 1000 fibers per mouse counted. (**J**) Fiber area distribution quantified from H&E-stained histological sections from the quadriceps in the indicated genotypes of mice at 6 months of age. At least 600 fibers were counted total from five separate mice each. $^*P < 0.05$ versus Wt or $Mapk14^{fl/fl}$. Number of animals analyzed in each group is shown in the bars of each figure panel.

Myl1-cre knock-in allele. In a different line of mice, previous genetic targeting of *Mapk14* only resulted in a partial loss-of-function phenotype that produced viable mice with smaller skeletal muscle myofibers (10), although if targeted correctly, complete germline deletion of *Mapk14* is embryonic lethal (17,18). The loxP-targeted *Mapk14* line that we employed showed no effect on protein expression when homozygous, and we observed very efficient deletion of the gene product in skeletal muscle in the presence of the *Myl1-cre* allele, with a slight upregulation in total MKK6 protein (Fig. 1C). No deletion was observed in other tissues such as heart, liver and lung (data not shown). The *Myl1-cre* allele is commonly used to study the effects of gene deletion in mature myofibers. To demonstrate that the effects we observed in $Mapk14^{fl/fl\text{-}Myl1\text{-}cre}$ mice were not due altered myofiber development, we assessed the level of *Mapk14* deletion 1 week after birth. Western blot analysis revealed very little recombination of the *Mapk14* allele using the *Myl1-cre* driver at this early age (Supplementary Material, Fig. S1A). Gross histological examination of $Mapk14^{fl/fl\text{-}Myl1\text{-}cre}$ mice showed relatively normal overall muscle histology at 1, 3 and 6 months of age, although some central nucleation of myofibers was observed after 3 months (Fig. 1D and E and Supplementary Material, Fig. S1B and C). Central nuclei in myofibers can be due to increased activity of satellite cells during regeneration from previous myofiber loss. However, no other pathological indexes of disease were observed, such as fibrosis, increase in serum creatine kinase (CK) levels, or a reduction in running performance/endurance of the mice (Fig. 1F–H), suggesting that loss of *Mapk14* was not directly pathological. Embryonic myosin heavy chain re-expression is typically observed when new fibers are generated to replace dying fibers, but such expression was not observed in $Mapk14^{fl/fl\text{-}Myl1\text{-}cre}$ mice (data not shown), again suggesting that loss of p38α from skeletal muscle was not pathologic but likely was enhancing satellite cell activity or otherwise affecting the movement of central nuclei to the periphery of myofibers as they mature. Finally, as previously reported, we observed smaller fibers in skeletal muscle lacking *Mapk14* (10) in 6-month-old animals, as well as an increase in type I fibers that are part of the slow fiber-type program (Fig. 1I and J).

To examine the role of p38 signaling in muscle pathology, skeletal muscle-specific targeting of *Mapk14* was performed in the $Sgcd^{-/-}$ dystrophic background. Gross histological examination of quadriceps muscle sections showed a significant reduction in pathological indices in the $Mapk14^{fl/fl\text{-}Myl1\text{-}cre}$ $Sgcd^{-/-}$ mice compared with $Sgcd^{-/-}$ only control mice (Fig. 2A, Supplementary Material, Fig. S2A). Quadriceps and diaphragm muscle from $Sgcd^{-/-}$ mice showed the characteristic increase in central nucleation of myofibers, suggesting regeneration owing to continual degeneration, whereas this index was significantly reduced in $Sgcd^{-/-}$ with muscle-specific deletion of *Mapk14* (Fig. 2B, Supplementary Material, Fig. S2B). A marked reduction in interstitial fibrosis was also observed in the quadriceps and diaphragm muscle of $Mapk14^{fl/fl\text{-}Myl1\text{-}cre}$ $Sgcd^{-/-}$ mice compared with $Sgcd^{-/-}$ mice at both 3 and 6 months of age (Fig. 2C, Supplementary Material, Fig. S2C). Consistent with these histological features, $Mapk14^{fl/fl\text{-}Myl1\text{-}cre}$ $Sgcd^{-/-}$ mice performed significantly better with a forced treadmill running protocol compared with $Sgcd^{-/-}$ mice, suggesting improved muscle performance or endurance (Fig. 2D). However, deletion of *Mapk14* from $Sgcd^{-/-}$ mice did not lead to sustained improvements as mice continued to age up to and past 8 months of age, suggesting that the protection with deletion of p38α was attributed to a delay in disease progression (Supplementary Material, Fig. S3A–C).

Mice with muscle-specific targeting of the *Mapk14* gene in the $Sgcd^{-/-}$ background also showed a dramatic reduction in serum CK levels at 3 months of age and far less inflammation and macrophage recruitment to the quadriceps and diaphragm compared with $Sgcd^{-/-}$ mice, again demonstrating significantly less disease associated with loss of p38α at younger ages (Fig. 2E–G). However, instability of the myofiber sarcolemma in the quadriceps, as examined by Evan's blue dye (EBD) uptake in mice, still showed equally prominent leakiness between $Mapk14^{fl/fl\text{-}Myl1\text{-}cre}$ $Sgcd^{-/-}$ mice and $Sgcd^{-/-}$ mice, indicating that the underlying membrane defect owing to the loss of δ-sarcoglycan was still present, suggesting that the loss of p38α more specifically protected myofibers from degeneration (Fig. 2H, Supplementary Material, Fig. S4). No EBD-positive fibers were observed in control mice containing either *Myl1-cre* or $Mapk14^{fl/fl\text{-}Myl1\text{-}cre}$ alleles (Supplementary Material, Fig. S4 and data not shown). Thus, loss of p38α expression protected skeletal muscle from degeneration in the $Sgcd^{-/-}$ genetic background during the peak of disease (3–6 months).

We also crossed the $Mapk14^{fl/fl\text{-}Myl1\text{-}cre}$ alleles into the *mdx* genetic background to determine whether loss of p38α could similarly reduce muscle pathology in a second dystrophic mouse model owing to loss of dystrophin. As with the $Sgcd^{-/-}$ mice, we observed a marked decrease in the gross histopathology from quadriceps of $Mapk14^{fl/fl\text{-}Myl1\text{-}cre}$ *mdx* mice as compared with *mdx* only mice (Fig. 3A, Supplementary Material, Fig. S5A). Central nucleation and fibrosis in the *mdx* background was also significantly reduced with muscle-specific deletion of *Mapk14* in the quadriceps and the diaphragm at 3 and 6 months of age (Fig. 3B and C, Supplementary Material, Fig. S5B and C). We also assessed the levels of fibrosis and the proportion of myofibers with centrally located nuclei in *mdx* mice versus *mdx* mice lacking *Mapk14* and aged >1 year. We observed both significantly less central-nucleated fibers as well as a trend toward less fibrosis in either the quadriceps or diaphragm muscles of $Mapk14^{fl/fl\text{-}Myl1\text{-}cre}$ *mdx* mice compared with $Mapk14^{fl/fl}$ *mdx* mice (Supplementary Material, Fig. S6A–C). Muscle performance/endurance as measured by treadmill running was also improved in of the $Mapk14^{fl/fl\text{-}Myl1\text{-}cre}$ *mdx* mice compared with *mdx* only mice at 3 months of age (Fig. 3D, controls shown in Fig. 2D), and serum CK levels were significantly reduced at both 3 and 6 months of age by deletion of the *Mapk14* gene (Fig. 3E). Finally, the number of activated macrophages in quadriceps of $Mapk14^{fl/fl\text{-}Myl1\text{-}cre}$ *mdx* mice was also significantly reduced compared with *mdx* only (Fig. 3F). Hence, genetic deletion of *Mapk14* in the *mdx* background, which models the most common form of human muscular dystrophy, was similarly protective to the data generated in the $Sgcd^{-/-}$ background. Although, in both models of muscular dystrophy, the benefits associated with deletion of *Mapk14* appear to wane with age.

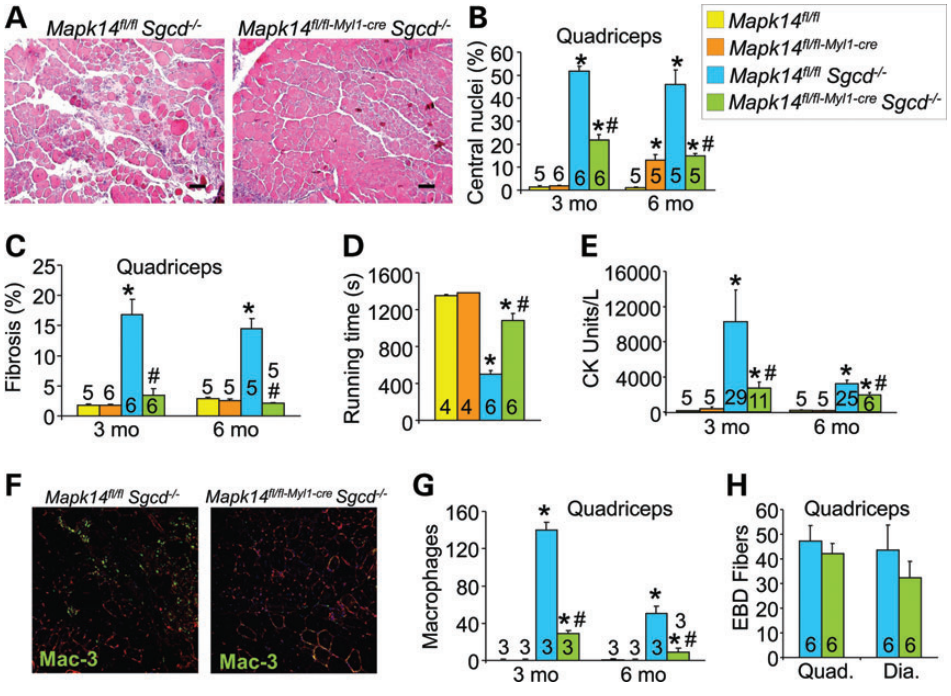

Figure 2. Genetic targeting of *Mapk14* in $Sgcd^{-/-}$ mice. (**A**) Representative H&E-stained histology of quadriceps from 3-month-old $Mapk14^{fl/fl}$ $Sgcd^{-/-}$ versus $Mapk14^{fl/fl\text{-}Myl1\text{-}cre}$ $Sgcd^{-/-}$ mice. Scale bars are 100 μm. (**B**) Percentage of fibers containing central nuclei in the quadriceps muscle of 3- and 6-month-old $Mapk14^{fl/fl}$, $Mapk14^{fl/fl\text{-}Myl1\text{-}cre}$, $Mapk14^{fl/fl}$ $Sgcd^{-/-}$ and $Mapk14^{fl/fl\text{-}Myl1\text{-}cre}$ $Sgcd^{-/-}$ mice. (**C**) Percentage of fibrotic area in histological sections from the quadriceps muscle of 3- and 6-month-old $Mapk14^{fl/fl}$, $Mapk14^{fl/fl\text{-}Myl1\text{-}cre}$, $Mapk14^{fl/fl}$ $Sgcd^{-/-}$ and $Mapk14^{fl/fl\text{-}Myl1\text{-}cre}$ $Sgcd^{-/-}$ mice. (**D**) Average time spent running on the treadmill in 3-month-old $Mapk14^{fl/fl}$, $Mapk14^{fl/fl\text{-}Myl1\text{-}cre}$, $Mapk14^{fl/fl}$ $Sgcd^{-/-}$ and $Mapk14^{fl/fl\text{-}Myl1\text{-}cre}$ $Sgcd^{-/-}$ mice. (**E**) Creatine kinase as units per liter found in the serum of 3- and 6-month-old $Mapk14^{fl/fl}$, $Mapk14^{fl/fl\text{-}Myl1\text{-}cre}$, $Mapk14^{fl/fl}$ $Sgcd^{-/-}$ and $Mapk14^{fl/fl\text{-}Myl1\text{-}cre}$ $Sgcd^{-/-}$ mice. (**F**) Representative immunohistochemical images for activated macrophages with Mac-3 antibody (green) from histological sections of the quadriceps in 3-month-old $Mapk14^{fl/fl}$ $Sgcd^{-/-}$ and $Mapk14^{fl/fl\text{-}Myl1\text{-}cre}$ $Sgcd^{-/-}$ mice. The red staining is for membranes with wheat-germ agglutinin (WGA)-TRITC. Magnification is 200×. Quantitation of these data (per imaged field with 20× objective) are shown in (**G**) along with control groups consisting of $Mapk14^{fl/fl}$ and $Mapk14^{fl/fl\text{-}Myl1\text{-}cre}$ mice at both 3 and 6 months of age. (**H**) Average number of positive EBD fibers in histological sections (per imaged field with 20× objective) from the quadriceps per field of view in 3-month-old $Mapk14^{fl/fl}$ $Sgcd^{-/-}$ and $Mapk14^{fl/fl\text{-}Myl1\text{-}cre}$ $Sgcd^{-/-}$ mice. $^{*}P < 0.05$ versus $Mapk14^{fl/fl}$; $^{\#}P < 0.05$ versus $Mapk14^{fl/fl}$ $Sgcd^{-/-}$. The number of mice used in each experiment is shown within the bars of each panel.

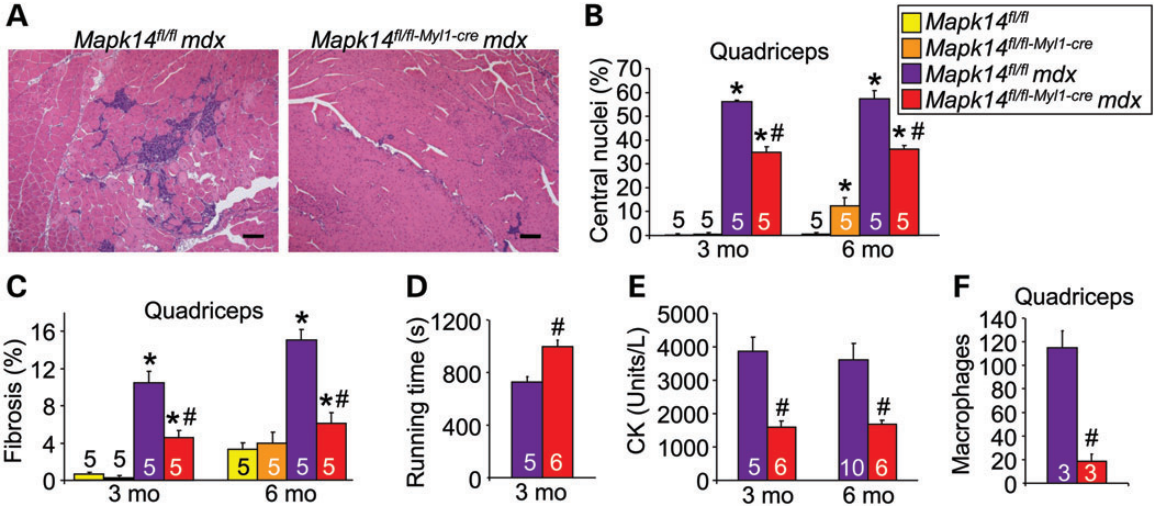

Figure 3. Genetic targeting of *Mapk14* in *mdx* mice. (**A**) Representative H&E-stained histology of quadriceps from 3-month-old $Mapk14^{fl/fl}$ *mdx* versus $Mapk14^{fl/fl\text{-}Myl1\text{-}cre}$ *mdx* mice. Scale bars are 100 μm. (**B**) Percentage of fibers containing central nuclei in the quadriceps muscle of 3- and 6-month-old mice of the indicated genotypes. (**C**) Percentage of fibrotic area in histological sections from the quadriceps muscle of 3- and 6-month-old mice of the indicated genotype. (**D**) Average time spent running on the treadmill in 3-month-old $Mapk14^{fl/fl}$ *mdx* and $Mapk14^{fl/fl\text{-}Myl1\text{-}cre}$ *mdx* mice. Control mice are shown in Fig. 2D. (**E**) Creatine kinase as units per liter found in the serum of 3- and 6-month-old $Mapk14^{fl/fl}$ *mdx* and $Mapk14^{fl/fl\text{-}Myl1\text{-}cre}$ *mdx* mice. (**F**) Average number of macrophages found per histological field (20× objective) from quadriceps in 3-month-old $Mapk14^{fl/fl}$ *mdx* and $Mapk14^{fl/fl\text{-}Myl1\text{-}cre}$ *mdx* mice. $^{*}P < 0.05$ versus $Mapk14^{fl/fl}$; $^{\#}P < 0.05$ versus $Mapk14^{fl/fl}$ *mdx*. Number of mice used in each study is shown within the bars of each panel.

Over-activation of p38α causes severe muscle-wasting pathology in mice

To determine whether p38 activation was itself sufficient to induce a pathologic response in skeletal muscle, we created a skeletal muscle-specific transgenic mouse model expressing a constitutively active form of MAPK kinase 6 (MKK6) under the control of the Human skeletal α-actin promoter (MKK6 Tg, Fig. 4A). Examination of skeletal muscle protein extracts from these transgenic mice showed a 7.8-fold increase in p38 phosphorylation status suggesting greater activity (Fig. 4B). Prominent histopathology was observed in all examined skeletal muscles from MKK6 Tg mice at 3 weeks, 3 and 6 months of age (Fig. 4C, Supplementary Material, Fig. S7A). Myofiber necrosis was so profound that muscle weights from the transgenic mice were severely reduced compared with Wt controls at 3 weeks, 3 months and 6 months (Fig. 4D and data not shown). A closer examination of the muscle histology of the MKK6 Tg mice showed large amounts of centrally nucleated myofibers, fibrosis, fatty tissue replacement and activated macrophage infiltration in the quadriceps and diaphragm at 3–4 weeks, 3 months and 6 months of age, indicating degenerating and regenerating muscle fibers owing to the MKK6 transgene (Fig. 4E–H, Supplementary Material, Fig. S7B and C). Analysis of embryonic myosin heavy chain protein expression indeed showed that despite the high levels of myofiber necrosis, newly formed regenerating fibers were present (Supplementary Material, Fig. S8). The data also show that regeneration was not induced by loss of *Mapk14* and hence not the reason for mild levels of persistent central nucleation shown in Figure 1D and E. Finally, ultrastructural analysis by transmission electron microscopy in skeletal muscle sections showed prominent mitochondrial swelling and rupture as early as 1 week after birth, and by 2 weeks, prominent necrotic fibers throughout the muscle were observed (Fig. 4I). Taken together, these data show that p38 activation in skeletal muscle is fully capable of inducing myofiber necrosis and a fulminant muscular dystrophy-like phenotype.

While MKK6 is functionally dedicated to p38 regulation, it was of concern that overexpression of this activated mutant protein might be inducing a muscular dystrophy-like phenotype independent of its regulation of p38α or that another p38 isoform (β,δ,γ) could be involved. To address this issue, we crossed MKK6 Tg mice with the muscle-specific *Mapk14*

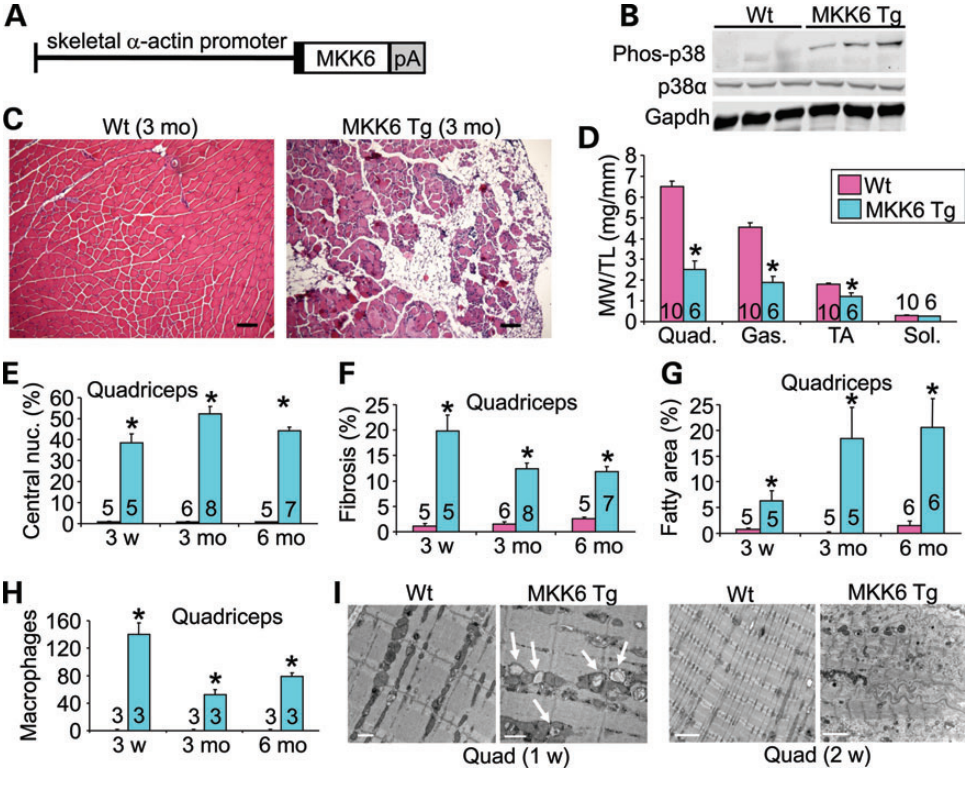

Figure 4. Skeletal muscle-specific mouse transgenic model with constitutive p38 activation. (**A**) Schematic of transgene construct used to make skeletal muscle-specific MKK6 Tg mice. pA represents the polyadenylation signal sequence. (**B**) Western blot p38 phosphorylation and total p38α from quadriceps of 1-week-old Wt and MKK6 Tg mice. Results from three separate mice are shown. (**C**) Representative H&E-stained histological sections from the quadriceps of 3-month-old Wt and MKK6 Tg mice. Scale bars are 100 μm. (**D**) Muscle weights (MW) of quadriceps, gastrocnemius, tibialis anterior and soleus from 3-month-old Wt and MKK6 Tg mice, normalized to tibia length (TL). (**E**) Percentage of fibers containing central nuclei from histological sections taken from quadriceps at 3-week, 3- and 6-month-old Wt and MKK6 Tg mice. (**F**) Percentage of fibrotic area in histological sections from quadriceps of 3-week, 3-month and 6-month-old Wt and MKK6 Tg mice. (**G**) Percentage of fatty replacement area in histological sections from quadriceps of 3-week, 3- and 6-month-old Wt and MKK6 Tg mice. (**H**) Average number of macrophages found per field (20× objective) of view from histological sections of quadriceps in 3-week, 3-month and 6-month-old Wt and MKK6 Tg mice. (**I**) Representative transmission electron micrographic images from quadriceps muscle of Wt and MKK Tg mice at 1 and 2 weeks of age. The white arrows show swollen and ruptured mitochondria. $^{*}P < 0.05$ versus Wt. Number of mice used in each study is shown with the bars of each panel.

deleted mice to determine whether the MKK6 Tg phenotype was solely due to p38α downstream signaling. Remarkably, *Mapk14*$^{fl/fl\text{-}Myl1\text{-}cre}$ MKK6 Tg mice showed a near-complete rescue in the muscular dystrophy-like disease state observed in MKK6 Tg mice at 1 and 6 months of age (Fig. 5A–D). Histological assessment from quadriceps and diaphragm of *Mapk14*$^{fl/fl\text{-}Myl1\text{-}cre}$ MKK6 Tg mice showed near-complete resolution of myofiber necrosis, irregular size distribution, inflammation, central myofiber nucleation and fibrosis that typifies the MKK6 Tg phenotype (Fig. 5A–D, Supplementary Material, Fig. S7B and C). Furthermore, we treated MKK6 Tg mice with the p38 inhibitor SB731445 (ref 19) for 4 weeks starting at 3 weeks of age. As early as 3 weeks of age, MKK6 Tg mice show dramatic pathology, which progresses with age.

In agreement with our genetic data, treatment of MKK6 Tg with SB731445 resolved the pathology present in MKK6 Tg animals (Supplementary Material, Figs S9A–E and S7). The proportion of myofibers with centrally located nuclei, fatty replacement and fibrosis was similar to Wt control littermates despite only 4 weeks of treatment initiated at weaning. Despite the rescue of muscle pathology by histological analysis, muscle weights did not recover over these 4 weeks of treatment (Supplementary Material, Fig. S9B). Overall our data show that the muscle pathology induced by the MKK6 transgene is entirely due to signaling through p38.

p38 induces myofiber necrosis and skeletal muscle disease through Bax

The most prominent disease feature in MKK6 Tg mice was the necrosis of myofibers and extreme loss of muscle mass, even at a very early age. Thus, we hypothesized that p38α was somehow directly regulating myofiber death in the context of muscular dystrophy, possibly by phosphorylating one more known cell death effectors. To this end, we first surveyed an array of known cell death effector proteins for changes in phosphorylation status from skeletal muscle of MKK6 Tg mice using the phos-tag electrophoresis system with subsequent western blotting (Fig. 6A). The most striking change was in the migration of Bax, suggesting that it was prominently phosphorylated by MKK6-p38 *in vivo*, whereas no migration changes were noted in other death-affecting proteins (Fig. 6A). However, we did observe increased protein content for Bcl-2, Bid, Bak, Bax, Arc and Xiap in muscle from MKK6 Tg mice at 3 weeks of age suggesting alterations in cell death signaling that were likely secondary and/or compensatory (Fig. 6A and B). The proapoptotic protein Bax was previously shown to be phosphorylated by p38 at threonine 167, which increased the cell death-promoting activity of this protein in cell culture (20–22). Use of a Bax-T167 phosphorylation-specific antibody confirmed its enhanced phosphorylation status in dystrophic muscle and MKK6 transgenic muscle (Fig. 6B and Supplementary Material, Fig. S10).

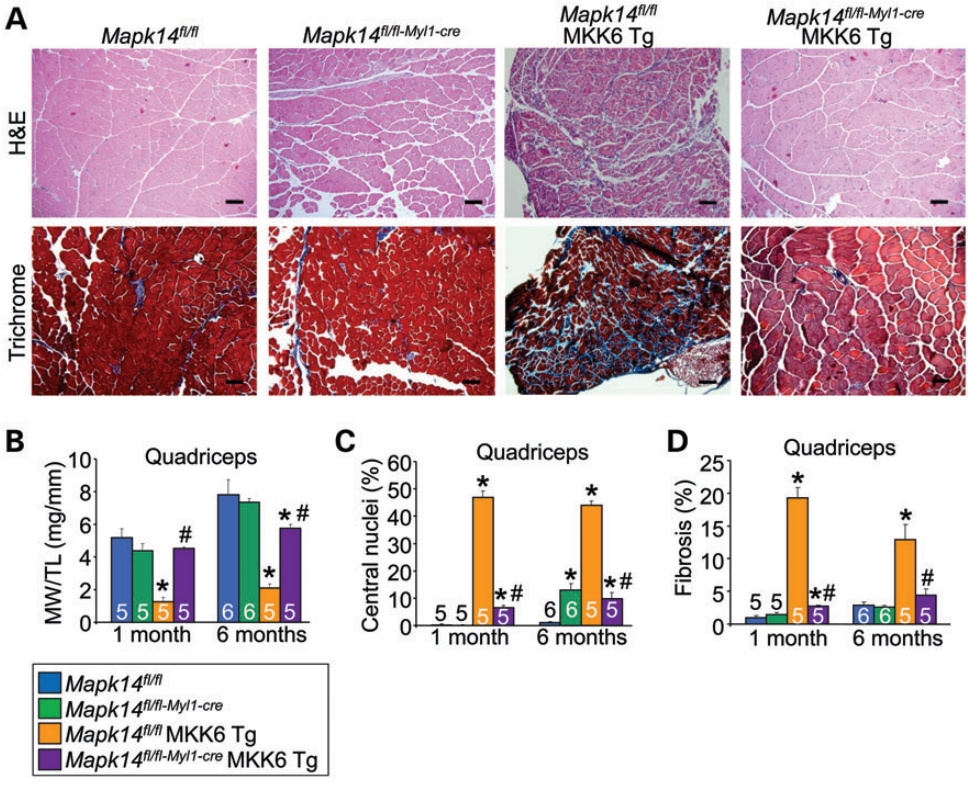

Figure 5. Rescue of MKK6 Tg phenotype by *Mapk14* deletion from skeletal muscle. (**A**) Representative H&E-stained and Masson's Trichrome-stained histological sections from quadriceps of 1-month-old *Mapk14*$^{fl/fl}$, *Mapk14*$^{fl/fl\text{-}Mly1\text{-}cre}$, *Mapk14*$^{fl/fl}$ MKK6 Tg and *Mapk14*$^{fl/fl\text{-}Mly1\text{-}cre}$ MKK6 Tg mice. Scale bars are 100 μm. (**B**) Percentage of fibers containing central nuclei from histological sections of the quadriceps in 1- and 6-month-old *Mapk14*$^{fl/fl}$, *Mapk14*$^{fl/fl\text{-}Mly1\text{-}cre}$, *Mapk14*$^{fl/fl}$ MKK6 Tg and *Mapk14*$^{fl/fl\text{-}Mly1\text{-}cre}$ MKK6 Tg mice. (**C** and **D**) Percentage of myofibers with central nuclei and fibrotic area in histological sections from the quadriceps of 1- and 6-month-old *Mapk14*$^{fl/fl}$, *Mapk14*$^{fl/fl\text{-}Mly1\text{-}cre}$, *Mapk14*$^{fl/fl}$ MKK6 Tg and *Mapk14*$^{fl/fl\text{-}Mly1\text{-}cre}$ MKK6 Tg mice. $^{*}P < 0.05$ versus Wt; $^{\#}P < 0.05$ versus *Mapk14*$^{fl/fl}$ MKK6 Tg. Number of mice analyzed is shown in the bars of each panel.

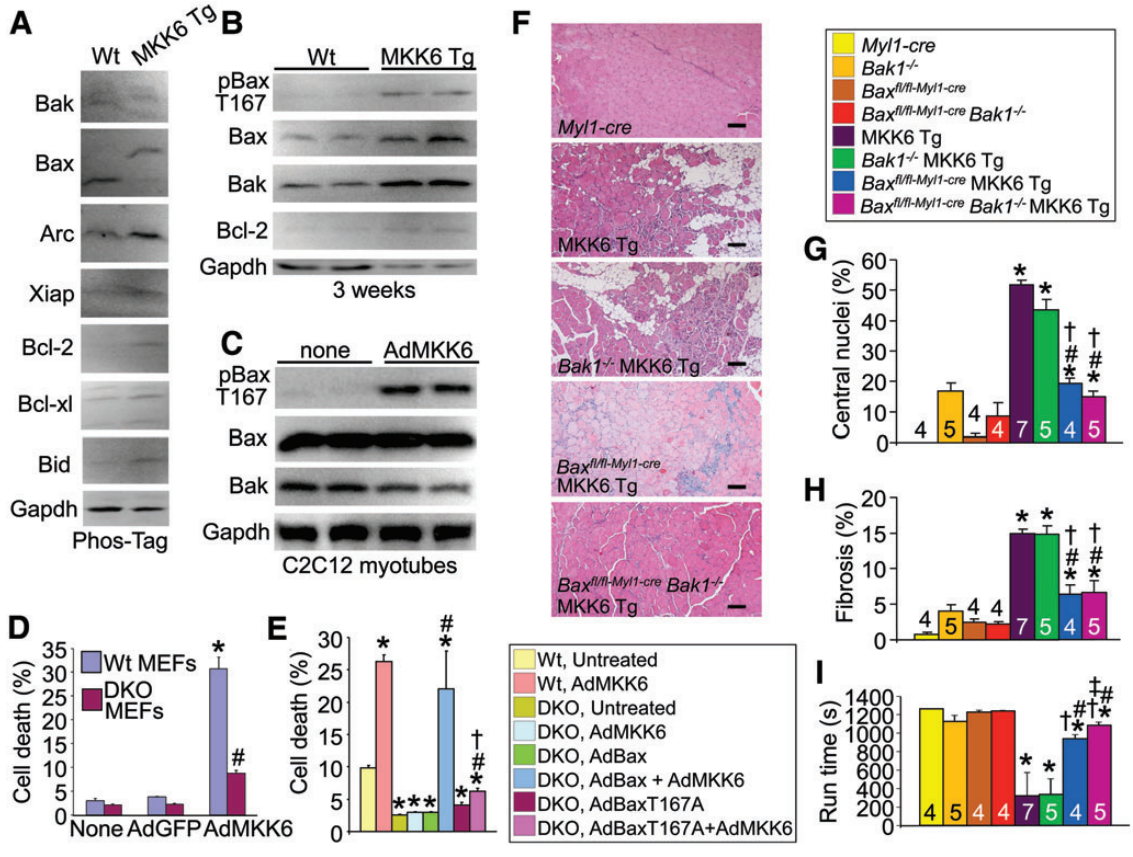

Figure 6. Enhanced Bax activity underlies skeletal muscle necrosis driven by MKK6-p38α signaling. (**A**) Western blots from Phos-tag PAGE to survey cell death-related proteins in quadriceps of 3-week-old Wt versus MKK6 Tg muscle. (**B**) Western blot using standard PAGE for the indicated proteins in quadriceps of 3-week-old Wt and MKK6 Tg mice. (**C**) Western blot of protein from C2C12 myotube extracts that were previously infected with AdMKK6 or no infection as a control. (**D**) Cell death assay in Wt MEFs and DKO MEFs (lacking *Bax/Bak1*) infected with AdMKK6, AdGFP or no virus. $^{*}P < 0.05$ versus Wt/DKO no virus; $^{\#}P < 0.05$ versus Wt AdMKK6. Results are from three independent experiments. (**E**) Cell death assay of Wt MEFs and DKO MEFs infected with no virus, AdMKK6, AdBax, AdBaxT167A, AdBax + AdMKK6 or AdBaxT167A + AdMKK6. $^{*}P < 0.05$ versus Wt untreated; $^{\#}P < 0.05$ versus DKO untreated; $^{\dagger}P < 0.05$ versus AdBax + AdMKK6. Results are from three independent experiments. (**F**) Representative H&E-stained histological sections from quadriceps of the indicated mice at 6 weeks of age. Scale bars are 100 μm. (**G**) Percentage of fibers with central nuclei from histological sections of the quadriceps of the indicated mice at 6 weeks of age. (**H**) Percentage of fibrotic area from histological sections of the quadriceps in the indicated mice at 6 weeks of age. (**I**) Average time spent running on the treadmill of 6-week-old mice as indicated in the legend box at the top right of the figure. $^{*}P < 0.05$ versus *Myl1-cre*; $^{\#}P < 0.05$ versus MKK6 Tg; $^{\dagger}P < 0.05$ versus *Bak1*$^{-/-}$ MKK6 Tg; $^{\ddagger}P < 0.05$ versus *Bax*$^{fl/fl\text{-}Myl1\text{-}cre}$ MKK6 Tg. Number of mice analyzed is shown in the bars of each panel.

Moreover, deletion of the *Mapk14* gene in the *mdx* background prevented Bax-T167 phosphorylation that is normally induced by muscular dystrophy (Supplementary Material, Fig. S10). Acute infection of C2C12 myotubes in culture with a recombinant adenovirus (Ad) expressing the activated MKK6 mutant (AdMKK6) showed high levels of Bax-T167 phosphorylation with almost no baseline phosphorylation in control uninfected cultures (Fig. 6C).

To investigate the potential mechanistic effects of p38-mediated phosphorylation of Bax in regulating cell death, we employed mouse embryonic fibroblasts (MEFs) deleted for *Bax* and *Bak1* (DKO) and compared them against Wt MEFs (23). These MEFs were first infected with AdMKK6, no virus or a control AdGFP (green fluorescent protein) and sorted by FACs for propidium iodide uptake to quantify cell death. Compared with Wt MEFs, DKO MEFs were resistant to cell death induced by AdMKK6, suggesting that p38 activation-induced cell death required Bax/Bak (Fig. 6D). AdMKK6 also prominently activated Bax protein, similar to staurosporine treatment, as assessed with a Bax conformation-dependent antibody (data not shown). To more directly implicate Bax, and specifically the phosphorylation of threonine 167 in Bax, we reconstituted DKO MEFs with Wt Bax or a mutant form of Bax that cannot be phosphorylated at T167 (Fig. 6E). The data show that reconstitution with Wt Bax restored AdMKK6-induced killing in the DKO MEFs, but not with the AdBaxT167A mutant (Fig. 6E). Western blotting confirmed expression from each of these adenoviruses and that AdBax and AdBaxT167A were expressed at comparable levels in the MEFs (Supplementary Material, Fig. S11A). These results indicate that phosphorylation of Bax-T167 is required to mediate the pro-cell death effects of MKK6-p38 signaling.

To investigate whether this mechanism holds true *in vivo*, we crossed the MKK6 transgene into the *Bax*$^{fl/fl\text{-}Myl1\text{-}cre}$ *Bak1*$^{-/-}$ genetic background. Previous work has shown that the deletion of *Bax* in the *Lama2*-deficient mouse background was sufficient

to reduce the severity of dystrophic disease and extend the lifespan of these mice (24,25). Analysis of histopathology and quantitation of disease showed that deletion of *Bak1* did not alleviate dystrophic disease owing to the MKK6 transgene, whereas deletion of *Bax* or the combined deletion of *Bax/Bak1* did produce dramatic improvement in skeletal muscle pathology with less central nucleation, fibrosis, inflammation, fatty replacement and TUNEL (Fig. 6F–H and data not shown, and Supplementary Material, Fig. S12A and B). Transmission electron microscopy confirmed these results and showed swollen mitochondria with sarcomeric disarray in skeletal muscle from MKK6 Tg mice, but deletion of *Bax* or double deletion of *Bak1/Bax* in the MKK6 Tg background noticeably improved mitochondrial morphology and sarcomeric structure, as well as a reduction in myofibers with ongoing necrosis (Supplementary Material, Fig. S11B). The MKK6 transgene also lead to augmented phosphorylation of Bax at T167 in muscle tissue *in vivo*, which was reduced when *Mapk14* was deleted (Supplementary Material, Fig. S11C). Assessment of muscle function by treadmill running was also consistent with the histopathology, as deletion of *Bak1* did not improve the poor performance/endurance of MKK6 Tg mice, whereas $Bax^{fl/fl\text{-}Myl1\text{-}cre}$ MKK6 Tg mice and $Bax^{fl/fl\text{-}Myl1\text{-}cre}$ $Bak1^{-/-}$ MKK6 Tg mice were significantly improved (Fig. 6I). These data suggest that loss of *Bax* or the combined disruption of *Bax/Bak1* reduced myofiber necrosis owing to MKK6-p38α signaling in skeletal muscle, further suggesting that one important mechanism whereby p38 activation contributes to muscular dystrophy is through regulation of Bax. As a control for this entire approach, we also deleted the *Tp53* gene, which encodes the tumor suppressor/apoptotic regulator p53 protein (Supplementary Material, Fig. S13). However, in this case, loss of p53, which typically lessens apoptotic cell death, was not protective in the MKK6 transgenic background, and in fact, appeared to worsen muscle disease leading to greater muscle weight loss (Supplementary Material, Fig. S13). Thus, the protection from MKK6-p38-driven muscle disease owing to loss of Bax is likely a more proximal mechanistic effect.

The results to this point suggested that a p38 pharmacologic inhibitor might have a therapeutic effect in models of muscular dystrophy. Hence, we instituted a drug treatment protocol in $Sgcd^{-/-}$ mice at two dosages of SB731445, 50 and 12.5 mg/kg/day. This inhibitor was previously shown to be highly specific for p38 MAPK inhibition and to have good pharmacokinetics *in vivo* (19). The treatment dosages used here resulted in similar blood levels of ∼200–350 ng/ml of drug, showing that the highest dosage was already saturating for drug uptake in the mouse. Mice were treated from 3 to 12 weeks of age with inhibitor-laden chow or vehicle chow (Fig. 7A). Treatment at both the high and low dose of SB731445 resulted in significantly less central nucleation of myofibers with less fibrosis in both the quadriceps and diaphragm of $Sgcd^{-/-}$ mice (Fig. 7B and C). Treatment with both dosages also reduced total CK levels at 12 weeks of age, as well as enhanced running time on the treadmill, with lower levels of tissue macrophage infiltration (Fig. 7D–F). In addition, we demonstrated that the levels of Bax-T167 phosphorylation in muscle from dystrophic $Sgcd^{-/-}$ mice was decreased following treatment with SB731445, again suggesting that p38 was directly involved in modulating Bax during the disease process (Fig. 7G). Thus, pharmacologic inhibition of p38 over 9 weeks significantly reduced dystrophic disease manifestation in juvenile $Sgcd^{-/-}$ mice.

DISCUSSION

p38 MAPK is a widely recognized activator of apoptosis in diverse cell types, but it has not been previously associated with myofiber death in muscular dystrophy. Our current work shows that p38 MAPK signaling is upregulated in two distinct mouse models of muscular dystrophy, indicating a possible role in over-activation of this MAPK family member in the progression of dystrophic disease. Loss of myofibers in muscular dystrophy is probably not due to classical caspase-dependent apoptosis, although effectors of apoptosis appear to be involved (26–31). Dying myofibers show a necrotic phenotype, and, while the term necrosis implies an unregulated default process, there are mounting data that many forms of necrosis are regulated (32). We have previously shown that Bax/Bak can regulate cellular necrosis through a direct effect on the outer mitochondrial membrane that is distinct from its mode of releasing cytochrome *c* in apoptosis (33). Bax/Bak impart a change in permeability of the outer mitochondrial membrane that permits necrosis through the mitochondrial permeability transition pore (MPTP), which is a regulated phenomenon that can directly lead to necrosis (33). Other studies by our group and others have shown that MPTP-dependent necrosis of myofibers is a prominent mechanism underlying the degeneration of skeletal muscle in muscular dystrophy (28,34). Thus, it would appear that loss of myofibers in muscular dystrophy is a regulated process, and the effectors underlying it could be targeted therapeutically. Indeed, Bax-dependent regulation of mitochondrial-driven cell death would appear to be a more nodal control point, although it is not clear how one would antagonize Bax or Bak. As stated earlier, the full pathogenesis of muscular dystrophy in *Lama2* gene-deleted mice was reduced by deletion of Bax, although overexpression of Bcl-2, which inhibits the activity of Bax/Bak, did not reduce pathogenesis in *mdx* mice (24). Here, we showed that p38 signaling directly activates Bax by phosphorylation at T167 in skeletal muscle to enhance its cell death-promoting functions. Loss of *Bax*, but not *Bak1*, antagonized the extent of skeletal muscle necrosis and ensuing histopathology observed in MKK6 transgenic mice, whereas loss of a different pro-death factor, p53, had no effect suggesting a more proximal disease effect through Bax.

However, it is also possible that MKK6-p38 influence the death of myofibers in muscular dystrophy through other effectors, as deletion of *Bax/Bak1* did not fully rescue skeletal muscle disease in MKK6 transgenic mice. Moreover, inhibition of p38 may be protective to skeletal muscle independent of myofiber death, such as by affecting the differentiation status of skeletal muscle (35), or even by reducing the fibrotic response mediated by surrounding fibroblasts (36). Indeed, data in myotube cultures and in hypomorphic *Mapk14* gene-deleted mice (using the epiblast-specific MORE-cre allele) would suggest that p38 inhibitors might antagonize regeneration of myofibers in muscular dystrophy, which should exacerbate disease (10). However, the *Myl1-cre* knock-in allele that was employed to delete *Mapk14* is not active in satellite cells, so in our model, p38 loss should not directly affect regeneration of skeletal muscle or its early development. Therefore, the protection conferred by p38 loss in the data presented here is most likely due to decreased myofiber necrosis without affects from satellite cells. Taking into account all of these considerations,

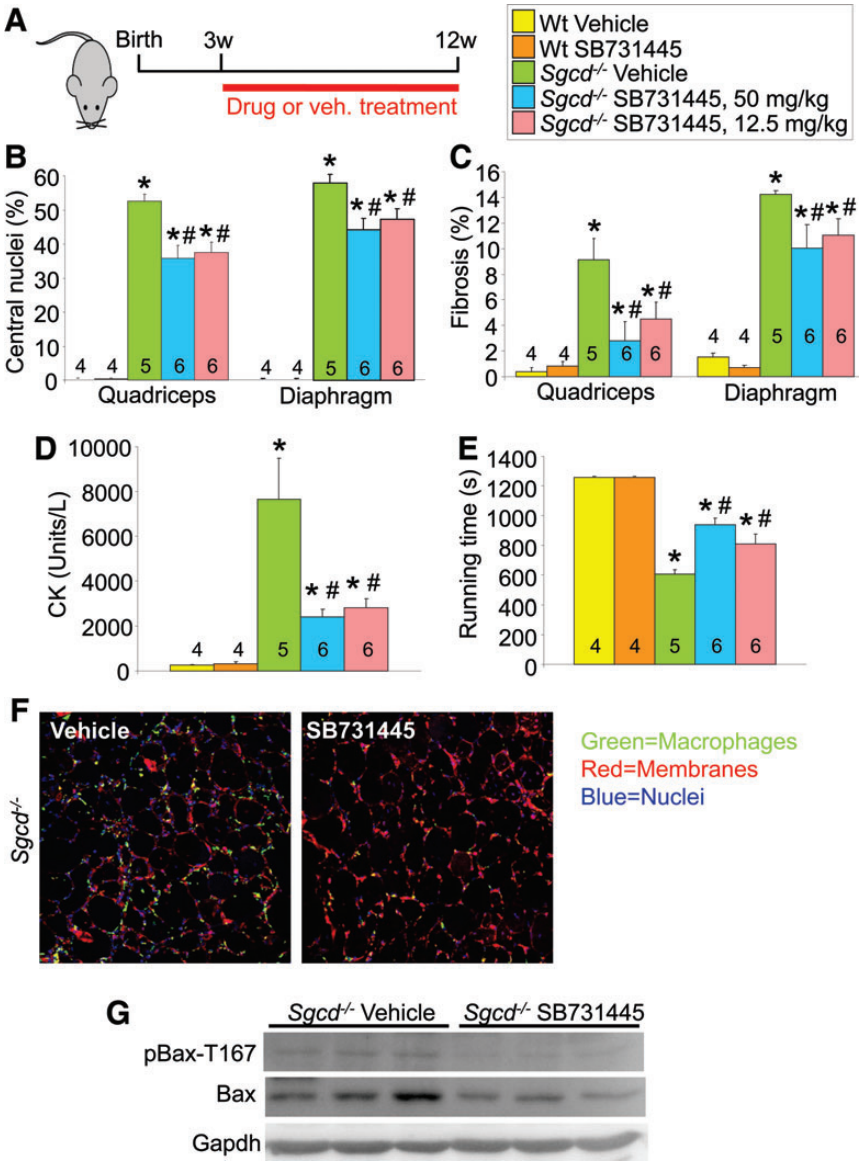

Figure 7. Pharmacological inhibition of p38 in $Sgcd^{-/-}$ mice. (**A**) Schematic of the SB731445 treatment regimen in Wt or $Sgcd^{-/-}$ mice with formulated chow at 50 mg/kg/day or 12.5 mg/kg/day versus vehicle chow. (**B**) Percentage of fibers containing central nuclei from histological sections taken from quadriceps and diaphragm after 9 weeks of treatment with vehicle or inhibitor in $Sgcd^{-/-}$ or Wt mice. (**C**) Percentage of fibrotic area in histological sections taken from quadriceps and diaphragm after 9 weeks of treatment with vehicle or inhibitor in the indicated mice. (**D**) Creatine kinase as units per liter found in the serum of vehicle-, 50 mg/kg/day inhibitor- or 12.5 mg/kg/day inhibitor-treated $Sgcd^{-/-}$ or Wt mice. (**E**) Average time spent running on the treadmill in 9-week-treated Wt or $Sgcd^{-/-}$ given vehicle or inhibitor. (**F**) Representative immunohistological images for activated macrophages with Mac-3 antibody (green) (20× objective) from the quadriceps of 9-week-treated vehicle- and inhibitor-treated $Sgcd^{-/-}$ mice. The red staining is for membranes with WGA-TRITC. Magnification is 200×. $^{*}P < 0.05$ versus Wt vehicle-treated mice; $^{\#}P < 0.05$ versus $Sgcd^{-/-}$ vehicle-treated mice. The number of mice used in each experiment is shown within the bars of each panel. (**G**) Western blotting for the indicted proteins from muscle of $Sgcd^{-/-}$ mice treated with SB731445 or vehicle ($n = 3$ mice).

while pharmacologic p38 inhibitors may suggest an attractive new treatment to mitigate dystrophic pathology, it might not be mechanistically straightforward given antagonistic effects on satellite cells and regeneration (see below).

This same situation played out with the calcineurin inhibitory drug cyclosporine A, where the drug protected myofibers from degeneration, but at the same time, it inhibited the regenerative activity of the satellite cells (36). The disease protection we observed with SB731445 in $Sgcd^{-/-}$ mice from 3 to 12 weeks of age, when there is a very large degree of myofiber necrosis, suggests that a p38 inhibitor could be clinically meaningful. However, it is also possible that at other times in the disease when initial waves of necrosis have mostly abated and ongoing regeneration is more important, a p38 inhibitor would not be protective because of its effects on satellite cells. Indeed, while we did observe prominent protection in $Sgcd^{-/-}$ mice with SB731445, parallel studies in *mdx* mice and TO-2 hamsters showed mixed results with some pathologic indexes being reduced, but others not (data not shown). Moreover, some of the protection observed with *Mapk14* deletion in the

Sgcd$^{-/-}$ and *mdx* dystrophic backgrounds was lessened with more pronounced aging (8- and 12-month-old mice showed less protection), suggesting that the pathology sparring effect-associated p38 deletion delays the disease, similar to how prednisone currently works in Duchenne patients to delay disease. Additional future studies are clearly needed to determine how we might balance the use of a p38 inhibitor to reduce myofiber necrosis without impacting satellite cell activity, as well as to delay disease progression even more effectively. Indeed, p38 inhibitors are in clinical trials for various inflammatory-based disease indications and could be employed to treat muscular dystrophy patients if we understood the windows of treatment better or the type of dystrophic disease that would be most benefited (35,37,38).

MATERIALS AND METHODS

Ethics statement

All animal procedures and usage were approved by the Institutional Animal Care and Use Committee of the Cincinnati Children's Hospital Medical Center, protocol 2E11104. No human subjects were used or human tissue or cells.

Mice

Mapk14-loxP-targeted mice were described previously and are in the C57BL/6 background (39). *Sgcd*$^{-/-}$ were described previously and are also in the C57BL/6 background (40). *Bax-loxP*-targeted and *Bak1*-null mice (C567BL/6/SV129 background) were obtained from Jackson Laboratories as were *mdx* (C57BL/10) mice and control mice (C57BL/10). Mice expressing Cre recombinase under the control of the myosin light chain 1f (*Myl1*) genomic locus (knock-in) were provided by Steven Burden (Skirball Institute, NYU) and were previously described and are also in the C57BL/6 background (41). *Tp53*-null mice were obtained from Jackson Laboratories (C57BL/6/SV129 background). Constitutively active MKK6 transgenic mice (FVBN background) were generated by subcloning a constitutively active human MKK6 cDNA into the pcDNA3.1 vector driven by the human α-skeletal actin promoter (42). Only littermates were compared with the MKK6 Tg crossed into either the *Mapk14*- or *Bax/Bak1*-targeted backgrounds. Mice were sacrificed by isoflurane inhalation followed by cervical dislocation. The quadriceps and diaphragm muscles were excised and either snap-frozen or placed into 10% phosphate-buffered formalin for later analysis. Serum was taken for CK analysis. SB731445 was formulated in mouse chow (Research Diets) at two dosages to effectively treat mice at ∼12.5 or 50 mg/kg/day over 9 weeks. Both male and female mice were used.

Western blot analysis

Protein extracts were prepared from the quadriceps muscle by homogenization in cell lysis buffer (10 mM Tris–HCL (pH 7.5), 150 mM NaCl, 4% Glycerol, 0.5 M Na-Metabisulfite, 1% Triton X-100, 0.1% Na-Deoxycholate, 0.05% SDS) supplemented with dithiothreitol (1 mM), protease inhibitors (Roche) and phosphatase inhibitors (Roche). Protein extracts were run on SDS–PAGE or Phos-tag gels AAL-107 (Wako Pure Chemical Industries), transferred to a PVDF membrane and immunodetected as specified by the manufacturer (Amersham Biosciences). Antibodies used in this study were as follows: phospho-p38 (Cell Signaling, 1:1000 and Covance, 1:800), p38α (Cell Signaling, 1:1000), phospho-MK2 (amino acid 334, cell signaling, 1:800), MK2 (Cell Signaling, 1:800), MKK6 (Cell Signaling, 1:1000), MKK3 (Cell Signaling, 1:1000), Bax (Santa Cruz, 1:1000), Bak (Millipore, 1:500), Bid (Cell Signaling, 1:800), Bcl-2 (Santa Cruz, 1:500) Bcl-XL (Cell Signaling, 1:800), phospho-Bax (Abcam, 1:100), ARC (Caymen Chemical, 1:1000), Xiap (Cell Signaling, 1:1000), α-tubulin (Santa Cruz, 1:2500) and Gapdh (Fitzgerald Industries, 1:2500).

Pathological indices

Paraffin-embedded histological sections (5 μm) of skeletal muscle were prepared and stained with hematoxylin and eosin, or Masson's trichrome. Three pictures of each quadriceps or diaphragm muscle per mouse were taken, and the entire field of view was counted per mouse for analysis of central nucleation with ImageJ software (43). Percentage of fibrosis was analyzed using Metamorph 7.1 software (43,44). Masson's trichrome stain was also used to determine percentage of adipose tissue replacement ImageJ software. We analyzed the quadriceps from *Bak1*$^{-/-}$, *Bax*$^{fl/fl\text{-}Myl1\text{-}cre}$, *Bax*$^{fl/fl\text{-}Myl1\text{-}cre}$ *Bak1*$^{-/-}$, MKK6 Tg, *Bak1*$^{-/-}$ MKK6 Tg, *Bax*$^{fl/fl\text{-}Myl1\text{-}cre}$ MKK6 Tg and *Bax*$^{fl/fl\text{-}Myl1\text{-}cre}$ *Bak1*$^{-/-}$ MKK6 Tg mice for ultrastructural alterations by transmission electron microscopy as described previously (45).

Muscle functional assessment

Mice were subjected to forced treadmill running utilizing a ramping speed protocol as previously described (46). The time spent on the treadmill before exhaustion or the time taken to complete the protocol was recorded as 'average maximum time running'.

Immunohistochemistry and TUNEL

Slides were stained for Mac-3 and embryonic myosin heavy chain (eMyHC) as previously described (47). TUNEL (terminal deoxynucleotidyl transferase dUTP nick end-labeling) was performed on paraffin-embedded histological sections (5 μm) according to the manufacturer's protocol (*In situ* cell death detection kit, Roche). Myofibers were outlined using fluorescent staining for wheat-germ agglutinin (WGA)-TRITC, and the nuclei were visualized using TO-PRO3 nucleic acid stain (Invitrogen).

Evan's blue eye uptake

Mice were exercised using the ramping speed protocol at a 15° downward incline. EBD was injected (10 mg/ml in PBS) intraperitoneally (0.1 ml per 10 g body weight) 24 hours after training. The following day, the mice were subjected once more to the ramping speed protocol on the downward incline and, following completion of the protocol, were euthanized. Quadriceps muscle and diaphragm were embedded in Optimal Cutting Temperature Compound (Tissue-Tek) and frozen in liquid

nitrogen. Tissue sections were prepared (5 μm) and analyzed by fluorescent microscopy.

Adenoviruses

The MKK6 adenovirus was previously described (48). Adenoviruses for the inducible expression of Wt Bax and Bax-T167A mutant were generated using with AdenoX system (Clontech).

Cell death assay

SV40 Wt and *Bax/Bak1* double knock-out (DKO) MEFs were cultured in IMDM media (Fisher Scientific) supplemented with 10% bovine growth serum, 1% penicillin/streptomycin (Invitrogen) and 1% MEM Non-essential Amino Acids (Invitrogen). Cells were infected with adenovirus for MKK6, inducible Bax Wt or inducible Bax-T167A. Bax expression was induced with the addition 200 μM doxycycline. Forty eight-hours post-infection, cells were collected and stained (Biovisions); the proportion of live versus dying cells was determined by flow cytometry (BD LSRII).

Statistical analysis

The results are presented as means ± s.e.m. We used the student's two-tailed *t*-test to calculate significance. Values were considered significant if $P < 0.05$.

SUPPLEMENTARY MATERIAL

Supplementary Material is available at *HMG* online.

Conflict of Interest statement. None declared.

FUNDING

This work was supported by grants from the National Institutes of Health (J.D.M.) and the Howard Hughes Medical Institute (J.D.M.).

REFERENCES

1. Durbeej, M. and Campbell, K.P. (2002) Muscular dystrophies involving the dystrophin-glycoprotein complex: an overview of current mouse models. *Curr. Opin. Genet. Dev.*, **12**, 349–361.
2. Lapidos, K.A., Kakkar, R. and McNally, E.M. (2004) The dystrophin glycoprotein complex: signaling strength and integrity for the sarcolemma. *Circ. Res.*, **94**, 1023–1031.
3. Bansal, D., Miyake, K., Vogel, S.S., Groh, S., Chen, C.C., Williamson, R., McNeil, P.L. and Campbell, K.P. (2003) Defective membrane repair in dysferlin-deficient muscular dystrophy. *Nature*, **423**, 168–172.
4. Whitehead, N.P., Yeung, E.W. and Allen, D.G. (2006) Muscle damage in mdx (dystrophic) mice: role of calcium and reactive oxygen species. *Clin. Exp. Pharmacol. Physiol.*, **33**, 657–662.
5. Millay, D.P., Goonasekera, S.A., Sargent, M.A., Maillet, M., Aronow, B.J. and Molkentin, J.D. (2009) Calcium influx is sufficient to induce muscular dystrophy through a TRPC-dependent mechanism. *Proc. Natl. Acad. Sci. USA*, **106**, 19023–19028.
6. Chang, L. and Karin, M. (2001) Mammalian MAP kinase signalling cascades. *Nature*, **410**, 37–40.
7. Tibbles, L.A. and Woodgett, J.R. (1999) The stress-activated protein kinase pathways. *Cell. Mol. Life. Sci.*, **55**, 1230–1254.
8. Xia, Z., Dickens, M., Raingeaud, J., Davis, R.J. and Greenberg, M.E. (1995) Opposing effects of ERK and JNK-p38 MAP kinases on apoptosis. *Science*, **270**, 1326–1331.
9. Zhou, L., Opalinska, J. and Verma, A. (2007) p38 MAP kinase regulates stem cell apoptosis in human hematopoietic failure. *Cell Cycle*, **6**, 534–537.
10. Perdiguero, E., Ruiz-Bonilla, V., Gresh, L., Hui, L., Ballestar, E., Sousa-Victor, P., Baeza-Raja, B., Jardi, M., Bosch-Comas, A., Esteller, M. *et al.* (2007) Genetic analysis of p38 MAP kinases in myogenesis: fundamental role of p38alpha in abrogating myoblast proliferation. *EMBO J.*, **26**, 1245–1256.
11. Perdiguero, E., Ruiz-Bonilla, V., Serrano, A.L. and Munoz-Canoves, P. (2007) Genetic deficiency of p38alpha reveals its critical role in myoblast cell cycle exit: the p38alpha-JNK connection. *Cell Cycle*, **6**, 1298–1303.
12. Ruiz-Bonilla, V., Perdiguero, E., Gresh, L., Serrano, A.L., Zamora, M., Sousa-Victor, P., Jardi, M., Wagner, E.F. and Munoz-Canoves, P. (2008) Efficient adult skeletal muscle regeneration in mice deficient in p38beta, p38gamma and p38delta MAP kinases. *Cell Cycle*, **7**, 2208–2214.
13. Nakamura, A., Yoshida, K., Ueda, H., Takeda, S. and Ikeda, S. (2005) Up-regulation of mitogen activated protein kinases in mdx skeletal muscle following chronic treadmill exercise. *Biochim. Biophys. Acta.*, **1740**, 326–331.
14. Shi, H., Boadu, E., Mercan, F., Le, A.M., Flach, R.J., Zhang, L., Tyner, K.J., Olwin, B.B. and Bennett, A.M. (2010) MAP kinase phosphatase-1 deficiency impairs skeletal muscle regeneration and exacerbates muscular dystrophy. *FASEB J.*, **24**, 2985–2997.
15. Shi, H., Verma, M., Zhang, L., Dong, C., Flavell, R.A. and Bennett, A.M. (2013) Improved regenerative myogenesis and muscular dystrophy in mice lacking Mkp5. *J. Clin. Invest.*, **123**, 2064–2077.
16. Smythe, G.M. and Forwood, J.K. (2012) Altered mitogen-activated protein kinase signaling in dystrophic (mdx) muscle. *Muscle Nerve*, **46**, 374–383.
17. Adams, R.H., Porras, A., Alonso, G., Jones, M., Vintersten, K., Panelli, S., Valladares, A., Perez, L., Klein, R. and Nebreda, A.R. (2000) Essential role of p38alpha MAP kinase in placental but not embryonic cardiovascular development. *Mol. Cell.*, **6**, 109–116.
18. Tamura, K., Sudo, T., Senftleben, U., Dadak, A.M., Johnson, R. and Karin, M. (2000) Requirement for p38alpha in erythropoietin expression: a role for stress kinases in erythropoiesis. *Cell*, **102**, 221–231.
19. Page, T.H., Brown, A., Timms, E.M., Foxwell, B.M. and Ray, K.P. (2010) Inhibitors of p38 suppress cytokine production in rheumatoid arthritis synovial membranes: does variable inhibition of interleukin-6 production limit effectiveness *in vivo*? *Arthritis Rheum.*, **62**, 3221–3231.
20. Choi, S.Y., Kim, M.J., Kang, C.M., Bae, S., Cho, C.K., Soh, J.W., Kim, J.H., Kang, S., Chung, H.Y., Lee, Y.S. *et al.* (2006) Activation of Bak and Bax through c-abl-protein kinase Cdelta-p38 MAPK signaling in response to ionizing radiation in human non-small cell lung cancer cells. *J. Biol. Chem.*, **281**, 7049–7059.
21. Deacon, K., Mistry, P., Chernoff, J., Blank, J.L. and Patel, R. (2003) p38 mitogen-activated protein kinase mediates cell death and p21-activated kinase mediates cell survival during chemotherapeutic drug-induced mitotic arrest. *Mol. Biol. Cell.*, **14**, 2071–2087.
22. Kim, B.J., Ryu, S.W. and Song, B.J. (2006) JNK- and p38 kinase-mediated phosphorylation of Bax leads to its activation and mitochondrial translocation and to apoptosis of human hepatoma HepG2 cells. *J. Biol. Chem.*, **281**, 21256–21265.
23. Scorrano, L., Oakes, S.A., Opferman, J.T., Cheng, E.H., Sorcinelli, M.D., Pozzan, T. and Korsmeyer, S.J. (2003) BAX and BAK regulation of endoplasmic reticulum Ca2+: a control point for apoptosis. *Science*, **300**, 135–139.
24. Dominov, J.A., Kravetz, A.J., Ardelt, M., Kostek, C.A., Beermann, M.L. and Miller, J.B. (2005) Muscle-specific BCL2 expression ameliorates muscle disease in laminin {alpha}2-deficient, but not in dystrophin-deficient, mice. *Hum. Mol. Genet.*, **14**, 1029–1040.
25. Girgenrath, M., Dominov, J.A., Kostek, C.A. and Miller, J.B. (2004) Inhibition of apoptosis improves outcome in a model of congenital muscular dystrophy. *J. Clin. Invest.*, **114**, 1635–1639.
26. Honda, A., Abe, S., Hiroki, E., Honda, H., Iwanuma, O., Yanagisawa, N. and Ide, Y. (2007) Activation of caspase 3, 9, 12, and Bax in masseter muscle of mdx mice during necrosis. *J. Muscle Res. Cell Motil.*, **28**, 243–247.
27. Matsuda, R., Nishikawa, A. and Tanaka, H. (1995) Visualization of dystrophic muscle fibers in mdx mouse by vital staining with Evans blue:

evidence of apoptosis in dystrophin-deficient muscle. *J. Biochem.*, **118**, 959–964.
28. Millay, D.P., Sargent, M.A., Osinska, H., Baines, C.P., Barton, E.R., Vuagniaux, G., Sweeney, H.L., Robbins, J. and Molkentin, J.D. (2008) Genetic and pharmacologic inhibition of mitochondrial-dependent necrosis attenuates muscular dystrophy. *Nat. Med.*, **14**, 442–447.
29. Smith, J., Fowkes, G. and Schofield, P.N. (1995) Programmed cell death in dystrophic (mdx) muscle is inhibited by IGF-II. *Cell Death Differ.*, **2**, 243–251.
30. Tidball, J.G., Albrecht, D.E., Lokensgard, B.E. and Spencer, M.J. (1995) Apoptosis precedes necrosis of dystrophin-deficient muscle. *J. Cell Sci.*, **108** (Pt 6) 2197–2204.
31. Woo, M., Tanabe, Y., Ishii, H., Nonaka, I., Yokoyama, M. and Esaki, K. (1987) Muscle fiber growth and necrosis in dystrophic muscles: a comparative study between dy and mdx mice. *J. Neurol. Sci.*, **82**, 111–122.
32. Galluzzi, L., Vanden Berghe, T., Vanlangenakker, N., Buettner, S., Eisenberg, T., Vandenabeele, P., Madeo, F. and Kroemer, G. (2011) Programmed necrosis from molecules to health and disease. *Int. Rev. Cell. Mol. Biol.*, **289**, 1–35.
33. Karch, J., Kwong, J.Q., Burr, A.R., Sargent, M.A., Elrod, J.W., Peixoto, P.M., Martinez-Caballero, S., Osinska, H., Cheng, E.H., Robbins, J. *et al.* (2013) Bax and Bak function as the outer membrane component of the mitochondrial permeability pore in regulating necrotic cell death in mice. *Elife*, **2**, e00772.
34. Tiepolo, T., Angelin, A., Palma, E., Sabatelli, P., Merlini, L., Nicolosi, L., Finetti, F., Braghetta, P., Vuagniaux, G., Dumont, J.M. *et al.* (2009) The cyclophilin inhibitor Debio 025 normalizes mitochondrial function, muscle apoptosis and ultrastructural defects in Col6a1-/- myopathic mice. *Br. J. Pharmacol.*, **157**, 1045–1052.
35. Melloni, C., Sprecher, D.L., Sarov-Blat, L., Patel, M.R., Heitner, J.F., Hamm, C.W., Aylward, P., Tanguay, J.F., DeWinter, R.J., Marber, M.S. *et al.* (2012) The study of LoSmapimod treatment on inflammation and InfarCtSizE (SOLSTICE): design and rationale. *Am. Heart J.*, **164**, 646–653 e643.
36. Keren, A., Tamir, Y. and Bengal, E. (2006) The p38 MAPK signaling pathway: a major regulator of skeletal muscle development. *Mol. Cell Endocrinol.*, **252**, 224–230.
37. Elkhawad, M., Rudd, J.H., Sarov-Blat, L., Cai, G., Wells, R., Davies, L.C., Collier, D.J., Marber, M.S., Choudhury, R.P., Fayad, Z.A. *et al.* (2012) Effects of p38 mitogen-activated protein kinase inhibition on vascular and systemic inflammation in patients with atherosclerosis. *JACC Cardiovasc. Imag.*, **5**, 911–922.
38. Kyttaris, V.C. (2012) Kinase inhibitors: a new class of antirheumatic drugs. *Drug Des. Devel. Ther.*, **6**, 245–250.
39. Nishida, K., Yamaguchi, O., Hirotani, S., Hikoso, S., Higuchi, Y., Watanabe, T., Takeda, T., Osuka, S., Morita, T., Kondoh, G. *et al.* (2004) p38alpha mitogen-activated protein kinase plays a critical role in cardiomyocyte survival but not in cardiac hypertrophic growth in response to pressure overload. *Mol. Cell Biol.*, **24**, 10611–10620.
40. Hack, A.A., Lam, M.Y., Cordier, L., Shoturma, D.I., Ly, C.T., Hadhazy, M.A., Hadhazy, M.R., Sweeney, H.L. and McNally, E.M. (2000) Differential requirement for individual sarcoglycans and dystrophin in the assembly and function of the dystrophin-glycoprotein complex. *J. Cell Sci.*, **113** (Pt 14), 2535–2544.
41. Bothe, G.W., Haspel, J.A., Smith, C.L., Wiener, H.H. and Burden, S.J. (2000) Selective expression of Cre recombinase in skeletal muscle fibers. *Genesis*, **26**, 165–166.
42. Brennan, K.J. and Hardeman, E.C. (1993) Quantitative analysis of the human alpha-skeletal actin gene in transgenic mice. *J. Biol. Chem.*, **268**, 719–725.
43. Parsons, S.A., Millay, D.P., Sargent, M.A., McNally, E.M. and Molkentin, J.D. (2006) Age-dependent effect of myostatin blockade on disease severity in a murine model of limb-girdle muscular dystrophy. *Am. J. Pathol.*, **168**, 1975–1985.
44. Goonasekera, S.A., Lam, C.K., Millay, D.P., Sargent, M.A., Hajjar, R.J., Kranias, E.G. and Molkentin, J.D. (2011) Mitigation of muscular dystrophy in mice by SERCA overexpression in skeletal muscle. *J. Clin. Invest.*, **121**, 1044–1052.
45. Fewell, J.G., Osinska, H., Klevitsky, R., Ng, W., Sfyris, G., Bahrehmand, F. and Robbins, J. (1997) A treadmill exercise regimen for identifying cardiovascular phenotypes in transgenic mice. *Am. J. Physiol.*, **273**, H1595–e01605.
46. Wissing, E.R., Millay, D.P., Vuagniaux, G. and Molkentin, J.D. (2010) Debio-025 is more effective than prednisone in reducing muscular pathology in mdx mice. *Neuromuscul. Disord.*, **20**, 753–760.
47. Lorts, A., Schwanekamp, J.A., Baudino, T.A., McNally, E.M. and Molkentin, J.D. (2012) Deletion of periostin reduces muscular dystrophy and fibrosis in mice by modulating the transforming growth factor-beta pathway. *Proc. Natl. Acad. Sci. USA*, **109**, 10978–10983.
48. Kaiser, R.A., Bueno, O.F., Lips, D.J., Doevendans, P.A., Jones, F., Kimball, T.F. and Molkentin, J.D. (2004) Targeted inhibition of p38 mitogen-activated protein kinase antagonizes cardiac injury and cell death following ischemia-reperfusion *in vivo*. *J. Biol. Chem.*, **279**, 15524–15530.